Downlink Sensing in 5G-Advanced and 6G: SIB1-assisted SSB Approach

Moeinreza Golzadeh*, Esa Tiirola†, Lauri Anttila*, Jukka Talvitie*, Kari Hooli†, Oskari Tervo†, Ismael Peruga‡, Sami Hakola†, and Mikko Valkama*

*Tampere University, Tampere, Finland
†Nokia Corporation, Oulu, Finland
‡Work done while at Nokia

***Abstract*—This paper investigates the potential to leverage existing 5G NR signals for network-side integrated sensing and communications (ISAC). In general, the synchronization signal block (SSB) is a suitable candidate for always-on downlink sensing, due to its frequent periodical availability and because of its beam-sweeping nature. However, as this work demonstrates, using only the SSB has challenges related to radar ambiguity while being also limited in both distance and velocity resolution due to limited bandwidth and per-beam time duration, respectively. A novel solution is then introduced by combining SSB with downlink control information (DCI) and system information block 1 (SIB1) symbols. The corresponding implications and variants how SIB1 is optimized and configured are discussed, covering both 5G evolution and potential 6G solutions. The performance of the proposed approach is also assessed through realistic numerical evaluations at both 3.5 GHz and 28 GHz network deployments, and shown to yield up to 25 dB suppression in radar peak sidelobe level (PSL) compared to SSB-only based range-velocity profile. Also considerable improvements in the sensing resolution in the order of 120–190% are demonstrated.**

***Index Terms*—5G-Advanced, 6G, integrated sensing and communications, network as sensor, OFDM radar, radar ambiguity, SIB1, SSB.**

I. Introduction

The convergence of radar and communication systems is gaining a considerable momentum towards 5G-Advanced and sixth generation (6G) mobile communications [1]. To this end, the 3rd Generation Partnership Project (3GPP) SA1 group has developed a study item in Release 19 (Rel-19) dedicated to integrated sensing and communications (ISAC) [2], where the use cases and potential new system requirements are studied. In general, ISAC can be used either for communication-assisted sensing, where communication signals are exploited for sensing services, or sensing-assisted communications, where sensing is utilized to improve communications performance [1], [3]–[5]. Representative example use cases for radio-based sensing are environment monitoring, intelligent transportation, traffic monitoring, home security, and indoor health care [6].

The accelerated trend towards ISAC paradigm casts light on the adaptation of the 5G New Radio (NR) infrastructure to support sensing capabilities. Integration of radar into communication system can be realized in two flavours, depending on the spatial distribution of transmitters and sensing receivers – namely, the mono-static and bi/multi-static approaches [7]. The mono-static approach allows for sensing with only one base-station (BS) or next-generation Node B (gNB), where the transmitter (TX) and receiver (RX) are co-located and the radar functionality can in principle exploit the entire transmit waveform known to the receiver. However, an additional technical challenge in mono-static configuration is the self-interference stemming from the strong coupling of the transmit signal to the simultaneously operating receiver [8]–[10]. In bi-static or multi-static case, on the other hand, transmitter and receiver are geographically separated and the receiving nodes do not have, by default, the knowledge of the entire transmit signal. Hence, in this case, the commonly known reference signals or known synchronization signals serve as the physical sensing resource. When a user equipment (UE) is the receiving entity, such scenario is commonly referred to as bi-static downlink simultaneous localization and mapping (SLAM) [11] where the UE estimates its own location as well as the locations of the environment scattering points.

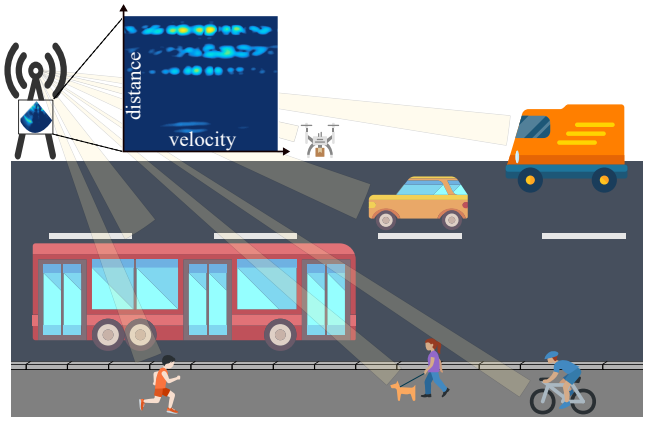

Fig. 1. Example downlink sensing scenario in an urban environment, with gNB receiving target reflections while performing 5G NR communications.

In general, new orthogonal frequency-division multiplexing (OFDM)-based or other waveforms optimized for sensing purposes have been studied and developed, see, e.g., [12]–[14]. Such approaches may, however, reduce the actual data communication capacity and/or impose large modifications to the 5G NR standards. Hence, reusing the current 5G NR signals imposes the minimal modifications to communication sub-system, assuming correct choice of signals for different sensing applications. This is the basic technical premise of this

work. Example candidate 5G NR physical signals in downlink (DL) include physical downlink shared channel (PDSCH), synchronization signals block (SSB), and physical downlink control channel (PDCCH) [15].

When it comes to the prior art in ISAC and physical-layer technology, [16] takes a deep dive into dynamic range and radar ambiguity for several candidate ISAC waveforms. Radar ambiguity using direct sequence spread spectrum (DSSS) signals is, in turn, studied in [17], while [18]–[21] proposed new waveform designs to improve radar peak sidelobes level (PSL). A correlation-based radar detection via SSB is suggested in [22], and in [23] SSB ambiguity function is derived for ISAC system. However, an open question remains whether DL sensing building on NR SSB can facilitate reliable and accurate target detection at different frequency ranges (FRs).

Motivated by above, the feasibility of SSB-based DL sensing is studied in this paper, with practical deployment emphasis under the current NR specifications. Additionally, and importantly, we also introduce an enhancement technique for DL sensing via jointly exploiting SSB, system information block 1 (SIB1), and downlink control information (DCI) which are all beamformed to the same direction. SIB1 and DCI are carried by PDSCH and PDCCH symbols dedicated to SIB1 message, respectively [15]. Additionally, they are transmitted in a beam-sweeping manner, thus allowing for good and periodical angular coverage for environment sensing. We describe different SIB1 optimization and configuration alternatives, allowing for either direct applications in 5G-Advanced networks or then paving the way towards the 6G standardization. We show through concrete numerical examples conforming to the current 5G NR specifications that substantial performance enhancements can be obtained through the proposed approach, at both 3.5 GHz and 28 GHz network deployments, compared to SSB-only based DL sensing.

The rest of this article is organized as follows. In Section II, the OFDM radar concept is shortly reviewed. Section III describes and compares the NR DL physical signals from their suitability to sensing at conceptual level. Additionally, the proposed SIB1-assisted sensing scheme and its different variants are described. In Section IV, comprehensive NR standard-compliant numerical results are presented, in an example case of gNB-based mono-static sensing, illustrating the performance advantages of the proposed method compared to ordinary SSB-only sensing. Finally, conclusions are drawn in Section V.

II. OFDM Radar System Model

Next, the OFDM radar processing principles, utilized to generate numerical results in Section IV, are shortly reviewed. For notational simplicity, we consider here the mono-static sensing case, while also omit the direct TX-RX coupling and the corresponding self-interference. To this end, the received signal after the gNB RX panel can be expressed as [10], [13]

$$r(t) = \sum_{k=0}^{K-1} b_k \, s(t-\tau_k) e^{j2\pi f_{D,k} t} + z(t) \tag{1}$$

where $s(t)$ is the time-domain transmit signal and $z(t)$ is additive white Gaussian noise (AWGN). Furthermore, K is the number of reflecting objects (targets), b_k is the effective two-way attenuation factor covering antenna gains, two-way propagation losses and the target radar cross section (RCS), while τ_k and $f_{D,k}$ are the two-way time delay and Doppler shift, respectively – all for target k. The corresponding frequency-domain model can be expressed as

$$(\mathbf{F}_{\text{RX}})_{p,q} = \sum_{k=0}^{K-1} b_k \, (\mathbf{F}_{\text{TX}})_{p,q} \, e^{j2\pi(qT_s f_{D,k} - p\tau_k \Delta f)} + (\mathbf{Z})_{p,q} \tag{2}$$

where $\mathbf{F}_{\text{RX}}, \mathbf{F}_{\text{TX}} \in \mathbb{C}^{M \times N}$ are the received and transmitted OFDM resource grids that span over M available subcarriers and N OFDM symbols, i.e., $p = 0, \ldots, M-1$, $q = 0, \ldots, N-1$. Furthermore, Δf is the subcarrier spacing (SCS), $T_s = 1/\Delta f + T_{cp}$ is the total time duration of one OFDM symbol, T_{cp} is the time duration of cyclic prefix, and finally $\mathbf{Z} \in \mathbb{C}^{M \times N}$ collects the frequency-domain AWGN samples.

The distances and relative velocities of the targets are the key parameters of interest, physically directly related to τ_k and $f_{D,k}$, i.e., the range-Doppler profile. They can be estimated, e.g., by the periodogram method [7], [13], that is based on element-wise division at active subcarriers with non-zero transmit samples, expressed as

$$(\mathbf{F})_{p,q} = \frac{(\mathbf{F}_{RX})_{p,q}}{(\mathbf{F}_{TX})_{p,q}} \tag{3}$$

where $\mathbf{F} \in \mathbb{C}^{M \times N}$ is the division outcome matrix. Afterwards, N_{per}-point fast Fourier transform (FFT) and M_{per}-point inverse FFT (IFFT) are applied to the division matrix. The generated range-velocity profile, denoted by $P_F(m,n)$, can be then expressed as

$$P_F(m,n) = \frac{1}{MN} \left| \sum_{p=0}^{M_{\text{per}}-1} \left(\sum_{q=0}^{N_{per}-1} (\mathbf{F})_{p,q} \, e^{-j2\pi \frac{qn}{N_{\text{per}}}} \right) e^{j2\pi \frac{pm}{M_{per}}} \right|^2 \tag{4}$$

where the range and velocity bins are indexed by $m = [0, \ldots, M_{\text{per}} - 1]$ and $n = [\, \lfloor \frac{-N_{\text{per}}}{2} \rfloor, \ldots, \lfloor \frac{N_{\text{per}}}{2} \rfloor - 1]$, respectively. In general, the different targets are present in the periodogram as the underlying peaks, hence implying an actual target detection stage where the chosen threshold impacts the radar's fundamental capabilities in terms of false alarm and missed detection probabilities. Additionally, and importantly, the ambiguity challenge related to detecting and separating two or more simultaneous targets is related to the utilized waveform [7].

Finally, the estimated distance $\hat{d}$ and the relative velocity $\hat{v}$ of a target at point $(\hat{m}, \hat{n})$ can be calculated as

$$\hat{d} = \frac{\hat{m}\, c_0}{2\, \Delta f \, M_{\text{per}}}, \;\; \hat{v} = \frac{\hat{n}\, c_0}{2\, f_c \, T_s \, N_{\text{per}}} \tag{5}$$

where c_0 is the speed of light and f_c is the transmit signal center frequency. The corresponding OFDM radar range resolution Δd and velocity resolution Δv can be expressed as

$$\Delta d = \frac{c_0}{2\, N_{\mathrm{SC}}^{\mathrm{act}}\, \Delta f}, \;\; \Delta v = \frac{c_0}{2\, T_{\mathrm{obs}} f_c} \tag{6}$$

where $N_{\mathrm{SC}}^{\mathrm{act}}$ is the number of active subcarriers and T_{obs} is the observation time duration. The angular resolution, in turn, depends on the number of available beamforming angles that the gNB antenna system allows for. In this paper, the SSB beam sweeping is realized by 8 and 64 separate azimuth angles at FR1 and FR2, respectively [24]. These are implementation feasible assumptions already in current 5G NR networks.

III. Proposed Method

A. Physical Signals

NR physical signals can, in general, be adopted for sensing according to their availability in the OFDM transmit grid, in terms of number of allocated subcarriers, number of OFDM symbols, and beam directions at which they are transmitted. As it is evident already from (6), large transmission bandwidths are a key enabler towards high resolution in range profile, while long time durations result in more accurate velocity profile. NR reference signals have commonly sparse time-frequency allocations compared to user data in PDSCH, impeding the range-velocity estimation. Thus, in the following, we discuss further only the applicability of PDSCH, SSB, and SIB1 as physical sensing signals. It is noted that demodulation reference signals (DMRSs) are also potential sensing resources – however, they are multiplexed with PDSCH and PDCCH signals and we thus do not treat them separately.

1) PDSCH: Large share of DL transmission resource across time and frequency is reserved for PDSCH symbols. For example, in DL-heavy slot format PDSCH occupies 12 OFDM symbols per slot and a maximum of 400 MHz bandwidth can be configured at FR2. Hence, from the time-frequency resouces point of view, PDSCH outperforms other candidate NR signals, however, being only applicable in mono-static sensing scenarios. Furthermore, beamformed PDSCH symbols are transmitted to certain directions where the communication users are present, and consequently, it results in poor target illumination capability in other directions. Additionally, allocation of PDSCH symbols is divided into non-contiguous parts in the grid, the so called Resource Block Groups (RBG), and target detection with combining results from sparse chunks of grid leads to a sub-optimal performance. Finally, PDSCH signal is available only when there is scheduling grant for users, and therefore *alternative always-on type of signals* are needed to initiate sensing in absence of communication users.

2) SSB: Fundamentally, each SSB consists of three parts: primary synchronization signal (PSS), secondary synchronization signal (SSS), and physical broadcast channel (PBCH) [15]. One SSB is 4 OFDM symbols long and spans over 20 physical resource blocks (PRB) in frequency domain, where the occupied bandwidth depends on SSB SCS, covering Cases A through G in the NR standard [24]. A synchronization signal

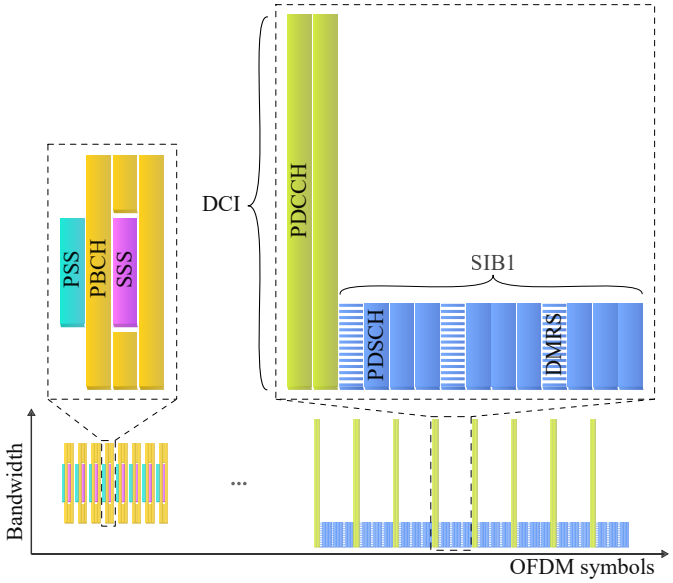

Fig. 2. Structure of SS burst *Case C* beamformed towards 8 directions, along with DCI in PDCCH and SIB1 in PDSCH.

(SS) burst comprises up to 8 and 64 SSBs with beam sweeping enabled at FR1 and FR2, respectively, and the burst duration is always confined to 5 ms. SS burst is transmitted periodically every 5 ms to 160 ms, depending on the network configuration, and during initial cell search users can assume the default periodicity of 20 ms. This always-on signal is broadcast over the complete cell area and sensing can thus be carried out regardless of communication users status. DL sensing via SSB can achieve a reasonable accuracy in range-angle estimation, thanks to the recurrent transmission in time compared to other NR reference signals. However, the accuracy of velocity estimation through only 4 OFDM symbols is not favourable, as illustrated also in the following section through numerical examples.

B. Proposed SIB1-Assisted Approach

The system information (SI) carried on SIB is necessary for communication devices (UEs) during cell search to establish proper connection to the network. Essential SI referred to as minimum SI builds upon two always-on signals: DCI with 80 ms periodicity and SIB1 with 160 ms periodicity. SIB1 is scheduled by DCI and is carried by PDSCH, while the DCI is carried by PDCCH. In the following, DCI term simply refers to the DCI which schedules SIB1.

In general, the communication users monitor for candidate PDCCHs on search spaces, by repetitively trying to decode PDCCH on the corresponding control resource sets (CORESET). Each CORESET block can be maximum 2 or 3 OFDM symbols long and this duration is determined whether PDSCH's front-loaded DMRS is located in the third or fourth symbol of a slot. However, in frequency domain, a CORESET is assigned to multiples of 6 PRBs and upper limited by the carrier bandwidth. CORESET0 is the first CORESET which is configured by MIB parameters and it contains the PDCCH

used to schedule the remaining minimum SI, that is, SIB1. A limited number of allocations are allowed for CORESET0 as it is configured with only a few bits in MIB while the possible configurations are provided in [24].

The gNB broadcasts DCI and SIB1 to the identical directions as in SSB beam sweeping, shown in Fig. 2. As a consequence, tailoring additional SIB1 symbols besides SSB symbols improves radar range and velocity estimation for a given direction in cell coverage area, due to the extension of both combined bandwidth and time duration. Radar range-angle and range-velocity profiles derived from SSB and SIB1 can be used interchangeably as a filter to resolve the estimation ambiguities. This is illustrated through numerical results in Section IV, together with the exact algorithmic approach how the different sets of OFDM symbols involved in the SIB1-assisted method are used to construct the final combined range-velocity and range-angle profiles.

C. 5G-Advanced vs. Potential 6G Variants

Next we describe different feasible implementation variants such that also bi-static/multi-static sensing is feasible, or that also UEs could participate in sensing in the form of downlink SLAM through the known transmit waveform. To this end, while the data in SSBs (including PSS, SSS, and PBCH) is considered static as a function of time, the data in SIB1 carrying, e.g., mandatory information on random access can vary over time. Hence, we foresee the following three variants described below.

1) Variant 1: SIB1s are assumed unchanged unless separately signaled. Such an approach is applicable to both 5G-Advanced and 6G. UEs can be informed, e.g., via a paging message while other gNBs can be informed by the available Xn-signaling. In this case, a UE can use every SIB1 for sensing, after the SIB1 has been decoded once – until receiving an indicator of an upcoming change. In general, gNB can configure SIB1 periodicity according to the prevailing sensing needs.

2) Variant 2: SIB1 is redefined such that information is divided in two segments – implying a potential 6G approach. The first segment contains unchanged information feasible for sensing, meaning that it is practically as stable as the information in PBCH. When changes are needed, system information update or cell reset can be performed. The second segment, in turn, contains variable information not used for sensing. Multiplexing of the first and second segments can be designed, e.g., to maximize the suitability for sensing, i.e., the first segment can be spread over the PDSCH bandwidth in a comb-like pattern.

3) Variant 3: SIB1s are assumed unchanged for a fixed predefined period. UEs participating in sensing are required to detect and decode SIB1 at the beginning of each new period. Other gNBs can be informed by Xn-signaling, when bi-static network sensing is pursued. SIB1 may contain parameters for SIB1 transmission periodicity that gNB follows for the period, as well as parameters defining the time period for static SIB1 (i.e., period and time offset).

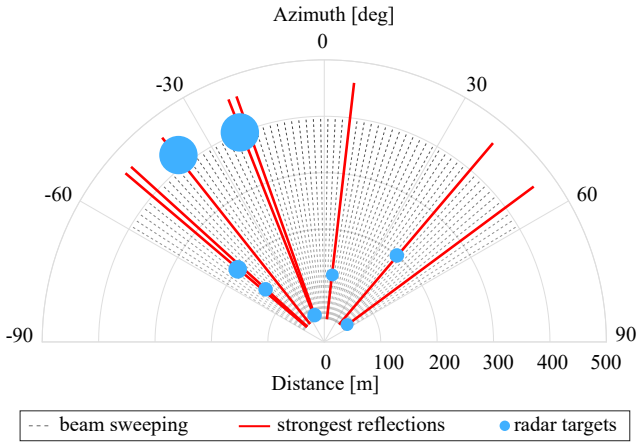

Fig. 3. Example radar scenario with 8 point targets, when transmitting beamformed SSB *Case D* towards 64 azimuth directions.

IV. Numerical Results

In this section, a collection of numerical results is provided, focusing for presentation simplicity on the single-gNB based mono-static sensing scenario. SSB-only based sensing approach forms the baseline reference, against which the proposed SIB1-assisted approach is then compared. Also fundamental sensing link budget results are provided.

A. Scenario and Assumptions

The considered sensing scenario contains 8 non-stationary radar targets moving across the sensing coverage area of the gNB-based ISAC system. Both 3.5 GHz and 28 GHz networks are considered with basic parameters such as the gNB effective isotropic radiated power (EIRP) and noise figure been shown along Table I. Signals are propagated in two-way LOS channel, per point target, assuming for visual simplicity that only a single reflection is received from every target and that there is no ground clutter. The non-fluctuating model [7] is assumed for the target RCS, with the numerical values being equal to $[1, 1, 2, 2, 2, 5, 30, 30]\,\mathrm{m}^2$ for the 8 targets. Small RCS values account for pedestrian and cyclist type of targets, while bigger RCS values model vehicles or trucks. The sensing scenario is graphically depicted in Fig. 3, considering that blue circles are radar targets spread across the sensing coverage zone and the size of the circles corresponds to target RCS values.

In order to construct a radar map from different azimuth directions, sufficient number of illuminating beams towards radar targets is required. The gNB TX and RX antenna panels are assumed to comprise 8×8 uniform rectangular arrays (URAs) at FR1 and 16×16 URAs at FR2. Cell angular coverage or sectorization is confined to operate within $[-60, 60]$ degrees in azimuth direction and the beam sweeping has angular spacing of 15° at FR1 and 1.8° at FR2. Periodogram runs with M_{per}-point IFFT and N_{per}-point FFT, selected as double the amounts of total number of transmitted OFDM symbols and total number of subcarriers in transmitted grid, respectively. In this study, the DL grid for a single beam sweep includes SSB with 4 OFDM symbols and 20 PRBs, DCI is

TABLE I

SENSING-RELATED LINK BUDGET CALCULATIONS FOR $\mathrm{SNR}_{min} = -10\,\mathrm{dB}$ AND $\mathrm{RSC} = 1\,\mathrm{m}^2$. NUMERICAL SENSING RESULTS ARE OBTAINED WITH THE SAME PARAMETER ASSUMPTIONS WHILE CONSIDERING THE EIRP NUMBERS HIGH-LIGHTED WITH GRAY SHADING.

Frequency	[GHz]	3.5						28					
G_{RX}	[dB]	18						24					
Noise figure	[dB]	3						7					
Δf	[kHz]	30			60			60			120		
Bandwidth	[MHz]	17.28			34.56			34.56			69.12		
Noise power	[dBm]	−98			−95			−91			−88		
EIRP	[dBm]	45	55	65	45	55	65	45	55	65	45	55	65
FSPL	[dB]	204	214	224	200	210	220	221	231	241	218	228	238
Max distance	[m]	**850**	**1500**	**2700**	**720**	**1280**	**2250**	**280**	**500**	**900**	**240**	**420**	**760**

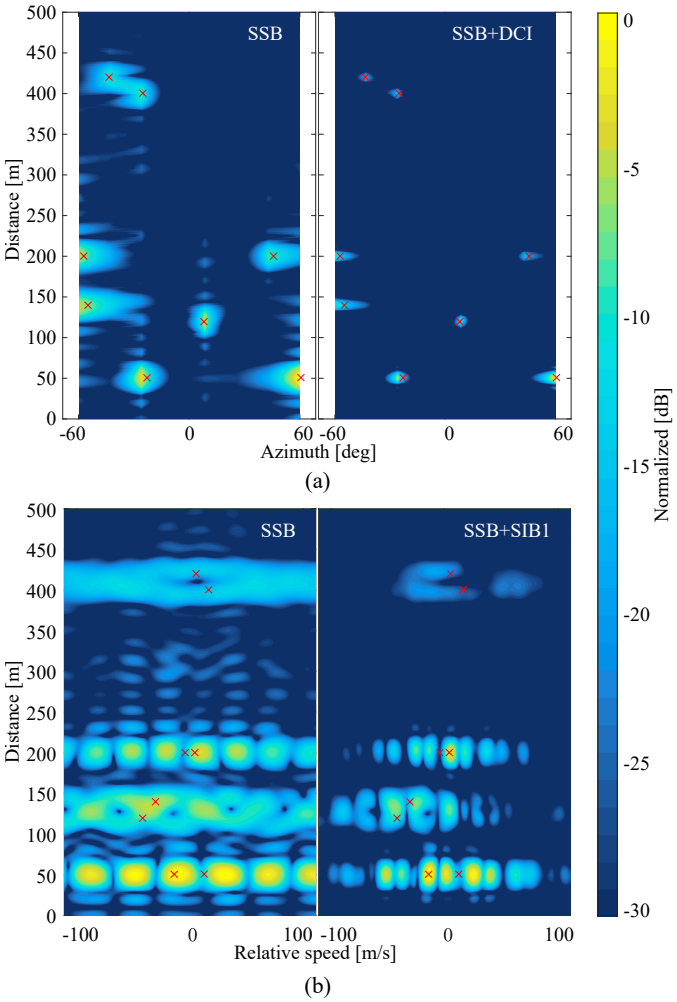

Fig. 4. Sensing results for the scenario with 8 point targets at 3.5 GHz. (a) range-angle profile, and (b) range-velocity profile, estimated from 8 SSB *Case C* compared with SSB+SIB1 combination.

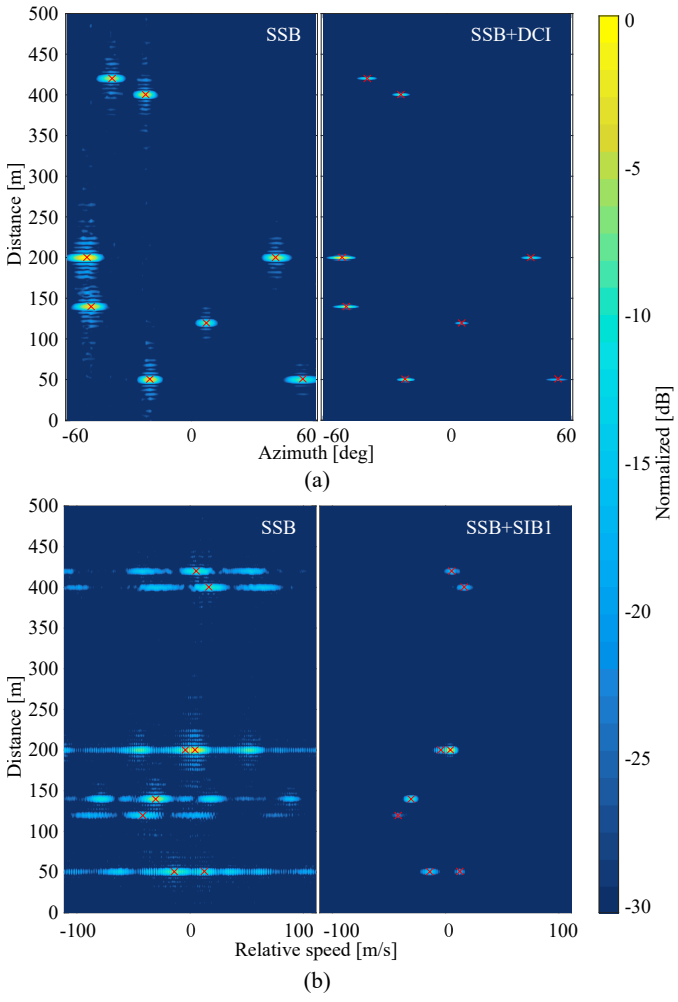

Fig. 5. Sensing results for the scenario with 8 point targets at 28 GHz. (a) range-angle profile, and (b) range-velocity profile, estimated from 64 SSB *Case D* compared with SSB+SIB1 combination.

assumed to be scheduled in 2 OFDM symbols and 48 PRBs, and SIB1 is allocated in 12 OFDM symbols and 8 PRBs. These 3 signals are multiplexed in time.

B. Link Budgets at FR1 and FR2

Before the actual sensing results, we shortly assess the feasible sensing distances through fundamental link budget calculations, focusing on the SIB1-assisted approach where the total resource grid contains SSB, DCI, and SIB1. The link budget results are presented in Table I, showing the maximum target distances as functions of SCS, gNB EIRP, thermal noise power, two-way free-space path loss (FSPL), target RCS, RX antenna gain (G_{RX}), and the needed minimum received signal-to-noise ratio (SNR_{min}) which is here assumed to be $-10\,\mathrm{dB}$

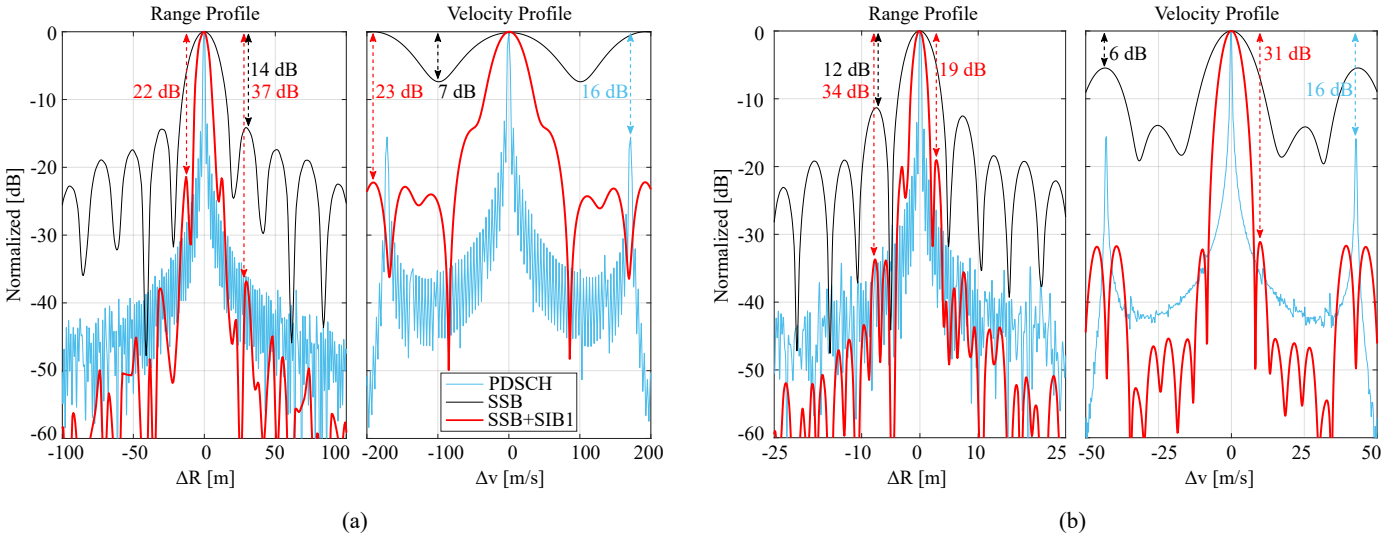

Fig. 6. Comparison of radar range and velocity profiles for different NR signals, when a single radar target is present. Carrier frequency is set to (a) 3.5 GHz and (b) 28 GHz. The SIB1-assisted approach offers largely improved radar profiles compared to ordinary SSB. The results with PDSCH carrying users data are also plotted for reference.

before the actual radar signal processing at RX [7]. Maximum transmitted power is set according to the DCI allocation, with 17.28 MHz and 69.12 MHz bandwidth at FR1 and FR2, respectively.

Based on the numerical results in Table I, the increased bandwidth of the SIB1-assisted approach (and thereon the increased noise power) does not essentially limit the sensing distances – even with low EIRP values of around +45 ... +55 dBm. In the following sensing experiments, we assume an EIRP of +45 dBm at FR1 and +65 dBm at FR2, respectively, such that all the targets shown in Fig. 3 are within the feasible sensing distance.

C. Sensing Results at FR1 and FR2

In the SIB1-assisted sensing processing, the range-angle profiles are calculated by means of combining the preliminary estimates out of two OFDM symbol sets: SSB with 4 OFDM symbols and DCI with 2 OFDM symbols. IFFT outcome forms a single range profile per beam sweep by summing up all 6 range profiles coherently across OFDM symbols. After element-wise multiplication of the obtained SSB and DCI profiles, the final results are obtained. Concrete illustrations are shown in Fig. 4(a) and Fig. 5(a) indicating a clearly improved range resolution at both frequency ranges, through the SIB1-assisted approach, when comparing against the ordinary SSB-based results. Similarly, the range-velocity enhancement is acquired by combining the OFDM symbol sets of SSB with 4 OFDM symbols and the slot carrying SIB1 with 14 OFDM symbols. SIB1 profile due to its longer time duration significantly improves the overall profile after performing element-wise multiplications of the SSB and SIB1 profiles. Fig. 4(b) and Fig. 5(b) further illustrate the achievable reduction in ambiguity level of the velocity profiles, especially in the FR2 case with denser beam sweeping.

Next, Fig. 6 illustrates the radar capabilities in terms of range ambiguity (ΔR) and velocity ambiguity (Δv) for a single point target, obtained with three NR signals: SSB, SSB+SIB1, and PDSCH for reference. The target is at 140 m distance from the gNB, moving at a relative velocity of 27 m/s. The PDSCH that is also shown for reference is configured with 20 consecutive DL-heavy slots in time domain, and it occupies 130 PRBs with 60 kHz SCS and 250 PRBs with 120 kHz SCS in the FR1 and FR2 cases, respectively. Each profile is a sinc-shaped function, with the peak value located at true distance or true velocity of the target. Contributing factors in the detection ambiguity include radar range-velocity resolution, radar PSL, and the distance of the sidelobes from the center of main lobe.

As can be observed through the range profiles in Fig. 6, the combination of SSB+DCI outperforms SSB-only with 23 dB of additional PSL suppression, followed by over 142% higher range resolution – interpreted here as the 3 dB mainlobe width – while the sidelobes appear at 30 m and 7 m away from the main lobe at FR1 and FR2, respectively. Moreover, the velocity profile of SSB+SIB1 obtained with 2 beams indicates 16 dB improved PSL and over 190% increased velocity resolution at FR1. Due to the higher number of beams at FR2, the reflections of 7 adjacent beams have constructive contribution in the velocity estimation. The velocity profile experiences over 25 dB of PSL improvement at FR2. The peak sidelobes are located at 120 m/s and 45 m/s away from the true velocity at FR1 and FR2, respectively. The obtained performance improvements in terms of PSL and resolution enhancements are summarized in Table II.

In this experiment, all the PDSCH symbols are deliberately beamformed towards the target location. As can be observed in Fig. 6, such beamformed PDSCH transmission results in narrowest target profiles among all the three signals. However,

TABLE II
SUMMARY OF THE SENSING PERFORMANCE IMPROVEMENTS USING THE PROPOSED METHOD, BUILDING ON THE COMBINATION OF SIB1 AND SSB

	Range		**Velocity**	
	PSL [dB]	Resolution	PSL [dB]	Resolution
FR1	+23	+142%	+16	+190%
FR2	+22	+145%	+25	+122%

this is applicable only when the target is at the same direction as the served UE. Extra sidelobes are also observed in the PDSCH velocity profile, being highlighted at -16 dB level in Fig. 6. The root cause of this phenomenon are the 2 empty OFDM symbols in the DL-heavy slot format that is assumed for PDSCH.

It should also be pointed out that if there exists empty OFDM symbols between DCI and SIB1, because of CORESET0 allocation and DMRS position of SIB1 in PDSCH, velocity estimation cannot fully leverage all 14 OFDM symbols per slot. As a consequence, phase discontinuity of the received signal creates extra sidelobes in velocity profile that is originating from the non-allocated OFDM symbols. Additionally, the accumulated velocity profile of SSB suffers from extra sidelobes, stemming from the symbol gap between contributing SSB signals.

V. CONCLUSION

This paper studied cellular sensing with particular emphasis on downlink and the use of NR built-in signals. The SSB is an always-on signal that is periodically available independent of the cell load and the amount of connected UEs, and is also transmitted in a beam-sweeping manner allowing for broad angular coverage. However, the time-frequency resourcing of SSB alone is limited in both bandwidth and time. Hence, a novel approach was proposed in this paper, building on the idea of jointly harnessing and combining the radar profiles of SSB with SIB1 and DCI, in order to enhance the sensing accuracy and reduce the ambiquity challenges related to the SSB alone. To support also sensing scenarios beyond the single-gNB based monostatic approach, different variants how SIB1 can be optimized and configured were also discussed, covering both 5G evolution and potential 6G solutions. Finally, concrete numerical examples and performance assessments were provided at both 3.5 GHz and 28 GHz bands, illustrating the quantitative benefits of the proposed approach. It was shown that the proposed SIB1-assisted approach allows to improve the sensing resolution by some 120–190%. Furthermore, the peak sidelobe levels of the range and velocity profiles were improved by 22–23 dB and 16–25 dB, respectively.

REFERENCES

[1] F. Liu, C. Masouros, A. P. Petropulu, H. Griffiths, and L. Hanzo, "Joint Radar and Communication Design: Applications, State-of-the-Art, and the Road Ahead," *IEEE Transactions on Communications*, vol. 68, no. 6, pp. 3834–3862, 2020.

[2] 3GPP Tech. Report 22.837, "Study on Integrated Sensing and Communication," *New SID, (Release 19)*, Feb. 2022.

[3] J. A. Zhang, M. L. Rahman, K. Wu, X. Huang, Y. J. Guo, S. Chen, and J. Yuan, "Enabling Joint Communication and Radar Sensing in Mobile Networks – A Survey," *arXiv:2006.07559*, 2020.

[4] A. Gameiro, D. Castanheira, J. Sanson, and P. P. Monteiro, "Research Challenges, Trends and Applications for Future Joint Radar Communications Systems," *Wireless Personal Communications*, vol. 100, pp. 81–96, 2018.

[5] C. Chaccour, M. N. Soorki, W. Saad, M. Bennis, P. Popovski, and M. Debbah, "Seven Defining Features of Terahertz (THz) Wireless Systems: A Fellowship of Communication and Sensing," *IEEE Communications Surveys & Tutorials*, vol. 24, no. 2, pp. 967–993, 2022.

[6] D. K. Pin Tan, J. He, Y. Li, A. Bayesteh, Y. Chen, P. Zhu, and W. Tong, "Integrated Sensing and Communication in 6G: Motivations, Use Cases, Requirements, Challenges and Future Directions," in *Proc. 2021 1st IEEE International Online Symposium on Joint Communications Sensing (JC&S)*, 2021, pp. 1–6.

[7] M. A. Richards, J. A. Scheer, and W. A. Holm, *Principles of Modern Radar: Basic principles*. Institution of Engineering and Technology, 2010.

[8] B. Paul, A. R. Chiriyath, and D. W. Bliss, "Survey of RF Communications and Sensing Convergence Research," *IEEE Access*, vol. 5, pp. 252–270, 2017.

[9] C. B. Barneto, S. D. Liyanaarachchi, M. Heino, T. Riihonen, and M. Valkama, "Full Duplex Radio/Radar Technology: The Enabler for Advanced Joint Communication and Sensing," *IEEE Wireless Communications*, vol. 28, no. 1, pp. 82–88, 2021.

[10] C. Baquero Barneto *et al.*, "Full-Duplex OFDM Radar With LTE and 5G NR Waveforms: Challenges, Solutions, and Measurements," *IEEE Transactions on Microwave Theory and Techniques*, vol. 67, no. 10, pp. 4042–4054, 2019.

[11] Y. Ge *et al.*, "A Computationally Efficient EK-PMBM Filter for Bistatic mmWave Radio SLAM," *IEEE Journal on Selected Areas in Communications*, vol. 40, no. 7, pp. 2179–2192, 2022.

[12] T. Wild, V. Braun, and H. Viswanathan, "Joint Design of Communication and Sensing for Beyond 5G and 6G Systems," *IEEE Access*, vol. 9, pp. 30 845–30 857, 2021.

[13] K. M. Braun, "OFDM Radar Algorithms in Mobile Communication Networks," Ph.D. dissertation, Karlsruher Institut für Technologie (KIT), 2014.

[14] S. D. Liyanaarachchi, T. Riihonen, C. B. Barneto, and M. Valkama, "Optimized Waveforms for 5G–6G Communication With Sensing: Theory, Simulations and Experiments," *IEEE Transactions on Wireless Communications*, vol. 20, no. 12, pp. 8301–8315, 2021.

[15] H. Holma, A. Toskala, and T. Nakamura, *5G Technology: 3GPP New Radio*. Wiley, 2019.

[16] C. Sturm and W. Wiesbeck, "Waveform Design and Signal Processing Aspects for Fusion of Wireless Communications and Radar Sensing," *Proceedings of the IEEE*, vol. 99, no. 7, pp. 1236–1259, 2011.

[17] L. Tang, K. Zhang, H. Dai, P. Zhu, and Y.-C. Liang, "Analysis and Optimization of Ambiguity Function in Radar-Communication Integrated Systems Using MPSK-DSSS," *IEEE Wireless Communications Letters*, vol. 8, no. 6, pp. 1546–1549, 2019.

[18] F. Liu, L. Zhou, C. Masouros, A. Li, W. Luo, and A. Petropulu, "Toward Dual-functional Radar-Communication Systems: Optimal Waveform Design," *IEEE Transactions on Signal Processing*, vol. 66, no. 16, pp. 4264–4279, 2018.

[19] R. Zhang, B. Shim, W. Yuan, M. D. Renzo, X. Dang, and W. Wu, "Integrated Sensing and Communication Waveform Design With Sparse Vector Coding: Low Sidelobes and Ultra Reliability," *IEEE Transactions on Vehicular Technology*, vol. 71, no. 4, pp. 4489–4494, 2022.

[20] M. F. Keskin, R. F. Tigrek, C. Aydogdu, F. Lampel, H. Wymeersch, A. Alvarado, and F. M. Willems, "Peak Sidelobe Level Based Waveform Optimization for OFDM Joint Radar-Communications," in *Proc. 2020 17th European Radar Conference (EuRAD)*, 2021, pp. 1–4.

[21] A. R. Chiriyath, S. Ragi, H. D. Mittelmann, and D. W. Bliss, "Novel Radar Waveform Optimization for a Cooperative Radar-Communications System," *IEEE Transactions on Aerospace and Electronic Systems*, vol. 55, no. 3, pp. 1160–1173, 2019.

[22] M. Kiviranta, I. Moilanen, and J. Roivainen, "5G Radar: Scenarios, Numerology and Simulations," in *Proc. 2019 International Conference on Military Communications and Information Systems (ICMCIS)*, 2019, pp. 1–6.

[23] Y. Cui, X. Jing, and J. Mu, "Integrated Sensing and Communications Via 5G NR Waveform: Performance Analysis," in *Proc. 2022 IEEE International Conference on Acoustics, Speech and Signal Processing (ICASSP 2022)*, 2022, pp. 8747–8751.

[24] 3GPP Tech. Spec. 38.213, "NR; Physical layer procedures for control," *v17.2.0, (Release 17)*, Jun. 2022.